Modelling order-disorder and magnetic transitions in iron-aluminium alloys

1992 J. Phys.: Condens. Matter 4 3569

(http://iopscience.iop.org/0953-8984/4/13/019)

J. Phys.: Condens. Matter 4 (1992) 3569–3588. Printed in the UK

Modelling order–disorder and magnetic transitions in iron–aluminium alloys

F Schmid and K Binder

Institut für Physik, Johannes Gutenberg-Universität Mainz, Staudingerweg 7, D-6500 Mainz, Federal Republic of Germany

Received 22 October 1991

Abstract. Information from recent x-ray and neutron diffuse scattering investigations of Fe–Al alloys and the resulting effective interaction parameters are used to construct a model in which the lattice configurational degrees of freedom of these alloys are described by Ising spins, and the magnetic moments of iron atoms are described by classical Heisenberg spins. Starting from the exact ground state of the model, information on the phase diagram at non-zero temperature is obtained from both spin wave theory, mean-field approximations and extensive Monte Carlo simulations. It is shown that use of the unrenormalized interaction parameters from the various experiments yields a phase diagram which disagrees severely with experiment even at the qualitative level. However, with a suitable renormalization of the ratio between magnetic and non-magnetic interactions, a qualitatively reasonable phase diagram of the model is obtained. The consequences for our understanding of effective interaction parameters in Fe–Al alloys are spelled out, and the implications for experimental work are discussed.

1. Introduction

The idea that order–disorder phenomena in binary alloys (AB) can be modelled by Ising spin degrees of freedom ($S_i = +1, -1$ means that lattice site i is occupied by an A or a B atom, respectively) has been exploited for a long time (for reviews, see for instance DeFontaine 1979, Binder 1986, Stocks and Gonis 1989, Inden and Pitsch 1991). Model descriptions in which phase diagrams are calculated from effective interatomic interaction parameters in the alloy are of interest for various purposes: as a test of 'first principles' electronic structure calculations of effective interaction parameters (e.g. Gautier *et al* 1975, Gyorffy and Stocks 1983, Turchi *et al* 1983, Bieber and Gautier 1984a,b, Gonis *et al* 1987, 1989, Carlsson 1987, 1988); for testing various methods of statistical mechanics, which always involve approximations or limitations that need to be explored (e.g. Binder 1980, 1981, 1986, Dünweg and Binder 1987, Kikuchi 1974, Kikuchi and van Baal 1974, Gahn 1982, 1986, Ackermann *et al* 1986, Diep *et al* 1986, Sanchez and DeFontaine 1978, 1980, 1982, Mohri *et al* 1985, Finel and Ducastelle 1986, Semenovskaya 1974, Khachaturyan 1978, Inden 1983, Inden and Pepperhoff 1990, Colinet *et al* 1992); and as a check of the self-consistency of effective interaction parameters derived from experiment (e.g. Gerold and Kern 1987, Schweika 1990, Pierron-Bohnes *et al* 1991a,b). Last, but not least, these models can be used to predict the physical properties of the alloy, for a range of parameters where experimental data are not yet available.

0953-8984/92/133569+20$04.50

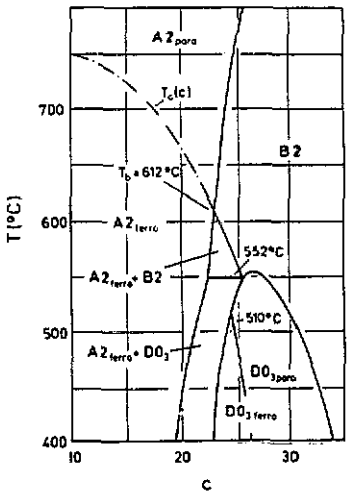

Figure 1. Part of the experimental phase diagram of Fe–Al alloys (from Kubaschewski 1982, in changed form). Only temperatures between 400 and 800 °C and Al concentrations c from 10 to 35 at.% are shown. All phases shown have the body-centered cubic (BCC) structure. The disordered solid solution (A2 phase, see figure 2, also denoted as α is paramagnetic for $T > T_c(c)$ and ferromagnetic for $T < T_c(c)$, $T_c(c)$ being shown as a chain line. At high temperatures ($612 < T < 1022$ °C) the paramagnetic A2 phase transforms into a paramagnetic B2 phase (FeAl structure, see figure 2) via a second-order transition. At $T_b = 612$ °C the ferromagnetic line $T_c(c)$ hits the A2–B2 order–disorder transition line in a bicritical point, for $552 < T < 612$ °C; hence a two-phase coexistence region occurs between the ferromagnetic α and paramagnetic FeAl phases. At 552 °C the (coherent) triple line involving the (paramagnetic) Fe_3Al phase of DO_3 symmetry (figure 2) occurs. At $T \lesssim 510$ °C the Fe_3Al phase exhibits a (second-order) transition to a ferromagnetic phase at sufficiently low iron concentrations. *Below $T \approx 400$ °C another phase (K1), the nature of which is controversial, occurs to* the left of the α–Fe_3Al coexistence range, and is not included here.

One of the classical alloy systems which has been of long-standing interest is that of the iron–aluminium alloy: its phase diagram (part of which we reproduce in figure 1) and ordering behaviour (figure 2) have been studied in detail (e.g. Bradley and Jay 1932, Thomas 1950, 1951, Davies 1953, Swann *et al* 1972, Okamoto and Beck 1971, Warliment and Thomas 1974, Allen and Cahn 1975, 1976, Allen 1977, Köster and Gödecke 1980, 1981, Schweika 1990, Pierron-Bohnes *et al* 1991a,b). Since iron is ferromagnetic, the iron-rich side of the phase diagram has complex and interesting magnetic properties (Nathans *et al* 1958, Pickart and Nathans 1961, Beck 1971, Shull *et al* 1976, Shiba and Nakamura 1976, Cable *et al* 1977, Shukla and Wortis 1980, Kuentzler 1983, Min *et al* 1986); only the ferromagnetic paramagnetic transition line is included in figure 1, while spin-glass-type phases are omitted (they would occur at a much lower temperature). The theoretical modelling of the order–disorder phenomena seen in figures 1 and 2 has also been of longstanding interest: applying mean-field approximations (Semenovskaya 1974, Sagane and Oki 1980), cluster variation techniques (Dünweg and Binder 1987, Contreras-Soloria *et al* 1988a,b, Colinet *et al* 1991) and Monte Carlo methods (Dünweg and Binder 1987, Inden and Pepperhoff 1990). These studies approximate the iron magnetic degree of freedom by an Ising spin and do not, as yet, include recent information on the interaction parameters extracted from scattering experiments (Schweika 1990, Pierron-Bohnes *et al* 1991a,b). Thus it

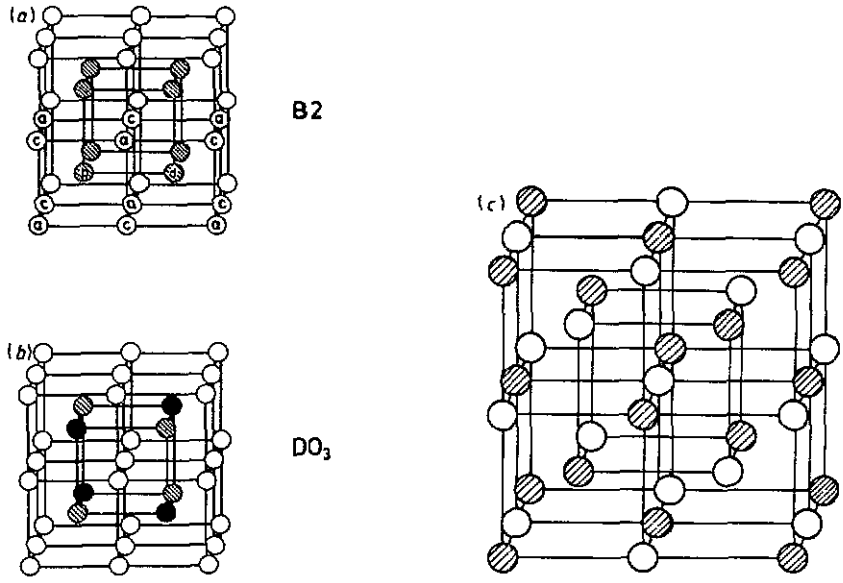

Figure 2. Part of the BCC lattice ordered (*a*) in the B2 structure; (*b*) the DO_3 structure; and (*c*) the B32 structure. (*a*) shows assignment of four sublattices a, b, c, d. In the A2 structure (not shown) the average concentration of A and B atoms is identical on all four sublattices, while in the B2 structure the concentrations of the b and d sublattices are the same, but differ from the concentration on the a and c sublattices, which again are the same. In the DO_3 structure, the concentrations of the a and c sublattices are still the same, while the concentration on sublattice b differs from the concentration on sublattice d. Finally, in the B32 phase the concentrations on sublattices a and b are the same, but differ from the concentrations on the c and *d* sublattices, which are then equal.

is no surprise that these studies have only a limited success in their description of ordering behaviour in Fe–Al alloys.

Hence the present work tackles this problem anew and is different in two important aspects from previous work:

(i) It takes into account the experimental fact that iron is nearly an isotropic ferromagnet, the magnetic degree of freedom is treated by the classical Heisenberg model rather than the Ising model.

(ii) The interaction parameters developed by Schweika (1990) and Pierron-Bohnes (1991a,b) are used as input for extensive Monte Carlo simulations.

Mean-field calculations are also carried out, but consistent with previous experience (e.g. Dünweg and Binder 1987) we find them very unreliable. We show that the naive use of these interaction parameters (taken together with an estimate of the magnetic exchange interaction extracted from $T_c(c = 0)$) yields phase diagrams which are inconsistent with observation. However, by suitably adjusting the ratio between magnetic and non-magnetic interaction parameters, a phase diagram is indeed found which—for the first time—has nicely reproduced all experimental features of the iron-rich side.

The outline of this paper is as follows: in section 2, we define the model and present its ground-state properties. Section 3 presents exact expansions, a second-order high-temperature expansion and at low temperatures a spin wave expansion.

These expansions provide valuable 'reference states', which are needed for the thermodynamic integration carried out in the context of our Monte Carlo work in order to estimate the location of first-order transitions precisely. In addition, a quantum-mechanical spin wave analysis is carried out (note that the Monte Carlo work deals with classical Heisenberg spins, spin quantum number $S \to \infty$, to assert the effects resulting from the fact that iron has spin quantum number $S = 1$). Section 4 presents the phase diagrams obtained from the Monte Carlo and mean-field calculations (technically, all these calculations are similar to those of Dünweg and Binder (1974); some comments on these techniques are summarized in the appendix). No cluster variation calculations were attempted—they are relatively laborious for alloys with Ising spins, and would be extremely cumbersome for Heisenberg spins. Section 5 presents a discussion and an outlook for further work.

Table 1. Experimental estimates for interaction parameters (in meV). No entry for V_4^{eff} means that V_4^{eff} was put equal to zero in the analysis.

		Source		
Interactions	Shell	Schweika (1990) $T = 1013$ K	Pierron-Bohnes *et al* (1991a) $T = 772$ K	Pierron-Bohnes *et al* (1991b) $T = 1473$–1573 K
V_1^{eff}	$(\frac{1}{2}\frac{1}{2}0)$	-17.5 ± 2	-5.4 ± 1.0	-12.0 ± 1.0
V_2^{eff}	(100)	-1.25 ± 2	-1.3 ± 0.5	-2.0 ± 0.5
V_3^{eff}	(110)	$+4.00 \pm 2$	$+5.0 \pm 0.5$	$+2.5 \pm 0.5$
V_4^{eff}	$(\frac{3}{2}\frac{1}{2}\frac{1}{2})$	$+2.00 \pm 2$	—	—
V_5^{eff}	(111)	≈ 0	$+0.2 \pm 0.5$	-0.7 ± 0.5

2. Model and ground-state analysis

As emphasized in the introduction, our model restricts attention to configurational and magnetic degrees of freedom; phonons, lattice distortions, etc are disregarded completely, and a perfect BCC lattice is assumed from the start. Representing the situation in which a lattice site i is occupied by a magnetic atom (Fe) by $S_i = +1$, while $S_i = -1$ indicates that i is occupied by a non-magnetic ion (Al), the Hamiltonian in the grand-canonical ensemble of the alloy is (cf, e.g., Binder 1986)

$$\mathcal{H} = -\frac{1}{2}\sum_{i \neq j} V_{ij} S_i S_j - \frac{1}{2}\sum_{i \neq j} J_{ij} \frac{(1+S_i)(1+S_j)}{4} \sigma_i \cdot \sigma_j - H \sum_i S_i. \tag{1}$$

Here σ_i is the unit vector in the direction of the spin representing the magnetic degree of freedom of the Fe ion; V_{ij} is the crystallographic interaction, J_{ij} the magnetic exchange interaction (which henceforth is restricted to nearest neighbours). The factors $\frac{1}{2}$ correct for overcounting the numbers of pairs (i, j). Note that $(1+S_i)/2 = c_i$ is nothing but the local concentration variable of Fe atoms. As is well known, V_{ij} is related to the pairwise interaction energies v_{ij}^{AA}, v_{ij}^{AB} and v_{ij}^{BB} of AA, AB and BB pairs in a binary alloy AB as $V_{ij} = -(v_{ij}^{\text{AA}} + v_{ij}^{\text{BB}} - 2v_{ij}^{\text{AB}})/4$. To avoid confusion, we stress that the 'field' H coupling the Ising spins is related to the chemical potential difference between the A and B atoms (see, e.g., Binder 1986); no real magnetic

field acting on the iron magnetic moments is included here. Also we have taken both V_{ij} and J_{ij} to be strictly independent of both the global concentration $\langle c_i \rangle$ and the local concentration of the nearest neighbours, also neglecting the possibility that an iron atom may lose some of its magnetic moment, if it has too many Al neighbours; see Beck (1971), Shukla and Wortis (1980) and Min *et al* (1986). Table 1 quotes the interaction parameters for the crystallographic interactions considered in this work. They were obtained from measurements at single crystals with an Al content of 20 at.% or 19.5 at.%, respectively, applying inverse Monte Carlo methods (Schweika *et al* 1990) and inverse cluster variation methods (Pierron-Bohnes *et al* 1991a,b) at the temperatures quoted. Apart from statistical errors (resulting mostly from the inaccuracy of the experimental data), there may be significant systematic errors due to the approximate consideration of the magnetic contributions: for a fully consistent treatment of the problem, one would have to study both crystallographic and magnetic short-range order simultaneously. This approximate treatment of magnetism in the analysis leading to table 1 (neglecting it in the paramagnetic region, assuming perfect alignment at $T = 772$ K) is particularly dangerous, since the magnetic exchange energy is somewhat large: using the high-temperature series estimate (Rushbrooke *et al* 1974) for the classical Heisenberg nearest-neighbour ferromagnet,

$$\frac{\frac{1}{2}J}{k_B T_c} = 0.2435 \tag{2}$$

together with the Curie temperature of pure Fe ($T_c = 1043$ K) yields

$$J = 43.7 \text{ meV} \tag{3}$$

while using the experimental estimates of the spin wave stiffness constant $\mathcal{D}$, $\mathcal{D} = 307 \pm 15$ meV Å^2 (Collins *et al* 1969) or $\mathcal{D} = 325 \pm 10$ meV Å^2 (Loong *et al* 1984) would yield

$$J = 37.2\text{–}39.5 \text{ meV}. \tag{4}$$

Here the spin wave energy $\hbar\omega_q$ is related to wavenumber q as $\hbar\omega_q = \mathcal{D}q^2 = Ja_0^2q^2$ at low temperatures, and the iron lattice constant $a_0 = 2.87$ Å is used. It is seen that equations (3) and (4) agree to within 10% accuracy, but are larger than the nearest-neighbour crystallographic energy (table 1). Here the effective interaction parameters V_l^{eff} are related to the V_l as $V_1^{\text{eff}} = V_1 + J/4$ ($T = 772$ K, ferromagnetic region) and $V_l^{\text{eff}} \equiv V_l$ in all other cases. Note that the highest temperatures considered in table 1 are close to the melting transition of the alloy, and it is conceivable that due to lattice expansion effects they are significantly different from those at the temperatures near the order–disorder transitions.

Motivated by the results shown in table 1, we first studied the following two models.

Model I: $V_1 = -17.5$ *meV.*

$$\begin{aligned} V_2/|V_1| &= -0.07 & V_3/|V_1| &= 0.23 & V_4/|V_1| &= 0.11 \\ V_5/|V_1| &= 0 & J/|V_1| &= 2.5 \end{aligned} \tag{5}$$

and

Model II: $V_1 = -16.3$ *meV.*

$$V_2/|V_1| = -0.081 \qquad V_3/|V_1| = 0.305 \qquad V_4 = V_5 = 0 \qquad J/|V_1| = 2.676. \tag{6}$$

Model I is based on the data of Schweika (1990) and model II on the data of Pierron-Bohnes *et al* (1991a). Since, as we shall see, these models cannot reproduce the Fe–Al system, we also studied a 'toy model' with weak magnetic interaction, namely model III, which is the same as model II, except that

$$J/|V_1| = 0.67. \tag{7}$$

Model IV, finally, was chosen on the basis of the high-temperature data of Pierron-Bohnes *et al* (1991b), with the ratio $J/|V_1|$ suitably adjusted:

$$V_2/|V_1| = -0.167 \qquad V_3/|V_1| = 0.208 \qquad V_4 = V_5 = 0 \qquad J/|V_1| = 1.65. \tag{8}$$

Within their uncertainties the experimental data would be compatible with various similar models, but this was not explored.

In the following we analyse the ground state of the model with general interactions V_1, V_2, V_3, V_4 and J. The ground-state energies per spin of the phases of interest are as follows (F stands for a ferromagnetic phase, P for a paramagnetic one):

$$\tfrac{1}{N}U^{(\mathrm{A2,F})} = -4J\ -4V_1\ -3V_2\ -6V_3\ -12V_4\ -H \tag{9a}$$
$$\tfrac{1}{N}U^{(\mathrm{DO_3,F})} = -2J\ -6V_3\ -\tfrac{1}{2}H \tag{9b}$$
$$\tfrac{1}{N}U^{(\mathrm{B2,P})} = +4V_1\ -3V_2\ -6V_3\ +12V_4 \tag{9c}$$
$$\tfrac{1}{N}U^{(\mathrm{B32,F})} = -J\ +3V_2\ -6V_3 \tag{9d}$$
$$\tfrac{1}{N}U^{(\mathrm{DO_3,P})} = -6V_3 \tag{9e}$$
$$\tfrac{1}{N}U^{(\mathrm{A2,P})} = -4V_1\ -3V_2\ -6V_3\ -12V_4\ +\tfrac{1}{2}H. \tag{9f}$$

It should be noted that the ground state contains the B2 phase if

$$J < -4V_1 + 6V_2 - 12V_4 \tag{10}$$

while otherwise the B32 phase occurs in the ground state. The A2(P,F) and DO_3(P,F) phases always occur at $T = 0$ for some ranges of the field H. The transition fields H_c between the various phases are found by equating the energies of the appropriate phases:

$$H_c^{(\mathrm{A2-DO_3,F})} = -4J\ -8V_1\ -6V_2\ -24V_4 \tag{11a}$$
$$H_c^{(\mathrm{DO_3,F-B2,P})} = -4J\ -8V_1\ +6V_2\ -24V_4 \tag{11b}$$
$$H_c^{(\mathrm{DO_3,F-B32,F})} = -2J\ -6V_2 \tag{11c}$$
$$H_c^{(\mathrm{B2,P-DO_3,P})} = +8V_1\ -6V_2\ +24V_4 \tag{11d}$$
$$H_c^{(\mathrm{B32,F-DO_3,P})} = -2J\ +6V_2 \tag{11e}$$
$$H_c^{(\mathrm{DO_3-A2,P})} = +8V_1\ +6V_2\ +24V_4. \tag{11f}$$

We will return to these results in the following sections.

3. Exact expansions

Exact expansions are carried out both at very high temperatures and at very low temperatures. These expansions are necessary for the following reasons:

(i) In order to locate first-order phase boundaries, the accuracy of Monte Carlo simulation data is limited by hysteresis. Precision can be improved by thermodynamic integration methods, however. For methods such as these (Binder 1981) it is very useful to have reference states at high and low temperatures, the free energy of which is known from other sources.

(ii) Comparing internal energies at the reference states and other observables obtained from the simulation with the exact expansion provides a very useful independent check on the Monte Carlo program.

(iii) At low temperatures the quantum nature of the iron magnetic moment is clearly important. It is straightforward to incorporate the quantum nature of the spin in the framework of the spin wave approximation to the Heisenberg model, while it would be very cumbersome to do this by quantum Monte Carlo methods.

3.1. High-temperature expansion

Here we only consider the expansion for the internal energy per lattice site. In principle the technique is a straightforward application of methods described by Domb (1974). Due to the relatively large range of the interaction and the simultaneous presence of crystallographic and magnetic interactions, the technique is rather tedious to apply, however, and hence only terms up to second order in $(k_B T)^{-1}$ are derived. Here we only quote the final result (for more details see Schmid 1991).

$$U = \langle \mathcal{H} \rangle / N = -(k_B T)^{-1} \left(H^2 + \frac{1}{2} \sum_j V_{0j}^2 + \frac{1}{24} \sum_j J_{0j}^2 \right) + \frac{1}{2}(k_B T)^{-2} \left\{ \sum_j \left(\frac{1}{8} V_{0j} J_{0j}^2 + 3H^2 V_{0j} + \frac{1}{4} H J_{0j}^2 \right) + \sum_{j \neq k \neq 0} \left(V_{0j} V_{jk} V_{ko} + \frac{1}{72} J_{0j} J_{jk} J_{ko} \right) \right\}. \tag{12}$$

Equation (12) holds for arbitrary lattices and for both crystallographic and magnetic interaction of arbitrary range (for the classical Heisenberg model). Specializing to the case where only four interaction parameters $\{V_l\} = \{V_1, V_2, V_3, V_4\}$ and the nearest-neighbour exchange are non-zero, as considered previously, the sums needed in equation (12) are, for the BCC lattice,

$$\sum_j V_{0j}^2 = 8V_1^2 + 6V_2^2 + 12V_3^2 + 24V_4^2 \tag{13a}$$

$$\sum_j J_{0j}^2 = 8J^2 \qquad \sum_j J_{0j} J_{jk} J_{ko} = 0 \tag{13b}$$

$$\sum_j V_{0j} J_{0j}^2 = 8V_1 J^2 \tag{13c}$$

$$\sum_j V_{0j} = 8V_1 + 6V_2 + 12V_3 + 24V_4 \tag{13d}$$

$$\sum_j V_{0j}V_{jk}V_{ko} = 72(V_1^2V_2 + V_1^2V_3 + 2V_1V_2V_4 + 4V_1V_3V_4 + V_2^3V_3 + 2V_2V_4^2 + 3V_3V_4^2 + \tfrac{2}{3}V_3^3). \tag{13e}$$

Figure 3 shows, in the spirit of point (ii), a comparison between equation (12) and corresponding Monte Carlo data. In our case it is seen that this second-order expansion is generally satisfactory for $|V_1|/k_BT \lesssim 0.1$, while the expansion to first order would only be accurate for $V_1/k_BT \lesssim 0.03$ in unfavourable cases.

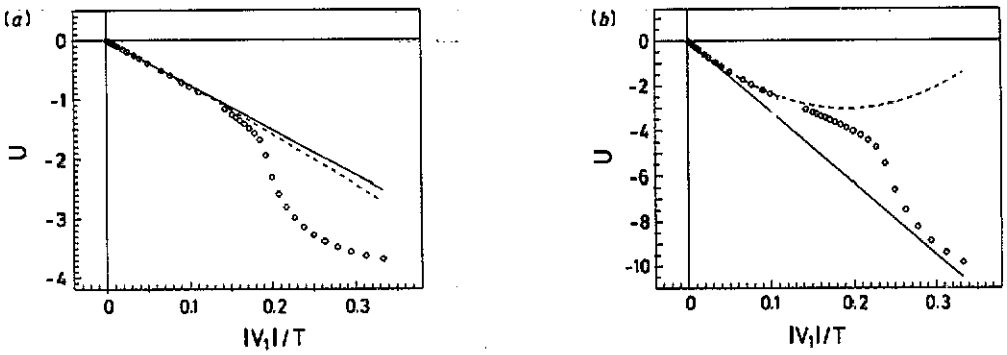

Figure 3. Plot of internal energy U per lattice site against inverse temperature, for the model with $V_2/|V_1| = -0.07$, $V_3/|V_1| = 0.23$, $V_4/|V_1| = 0.11$ and $J/|V_1| = 2.5$: (*a*) refers to $H/|V_1| = 1$; (*b*) to $H/|V_1| = 5$. Full and broken curves denote high-temperature series to first and second order, respectively, while circles show the Monte Carlo results.

3.2. Spin wave analysis: classical Heisenberg model

At low temperatures the overturning of an Ising degree of freedom relative to the ground-state Ising spin configuration can be disregarded, in comparison with the magnetic excitations. This is true because overturning an Ising spin always involves a non-zero excitation energy, at least if H differs from the critical values H_c considered in equation (11), while there is no gap in the spin wave spectrum; and thus there exist long-wavelength spin wave excitations of arbitrarily small excitation energy. They dominate the thermal behaviour at very low temperatures.

Consequently, we assume in the following that the crystallographic structure is perfect. Only the ferromagnetic A2, DO_3 and B32 phases need be considered (paramagnetic B2 and DO_3 phases are non-interacting ideal paramagnets in the framework of this description as $T \to 0$). While the ferromagnetic A2 phase (simple BCC Fe) amounts to a Bravais lattice, the two other structures do amount to non-Bravais lattices of the iron spins.

The Hamiltonian in the general case can be written as in non-interacting spin wave approximation

$$\mathcal{H} = \mathcal{H}_0 + \frac{1}{2}\sum_k \sum_{\alpha,\beta} A_k^{\alpha\beta}[\sigma_k^{\alpha x}\sigma_{-k}^{\beta x} + \sigma_k^{\alpha y}\sigma_{-k}^{\beta y}] \tag{14}$$

where α labels the sites in the basis cell of the (non-Bravais) lattice, and σ_k^α is the Fourier transform of the spin operator at site R_j^α

$$\sigma_k^\alpha = \frac{1}{\sqrt{\tilde{N}}} \sum_j \sigma_j^\alpha \exp(ik \cdot R_j^\alpha) \tag{15}$$

$\tilde{N}$ denoting the number of elementary cells in the system. The matrix $A_k^{\alpha\beta}$ in the presence of a magnetic field B coupling to the spins $\{\sigma_j^\alpha\}$ is given by

$$A_k^{\alpha\beta} = \left[\sqrt{\tilde{N}}\left(\sum_\gamma J_0^{\alpha\gamma}\delta_{\alpha\beta} - J_k^{\alpha\beta}\right) + B\delta_{\alpha\beta}\right] \tag{16}$$

$J_k^{\alpha\beta}$ being the Fourier transform of the exchange interaction between a spin at sublattice α and spins at sublattice β,

$$J_k^{\alpha\beta} = \frac{1}{\sqrt{\tilde{N}}} \sum_j J_{0j}^{\alpha\beta} \exp(ik \cdot R_j^\beta). \tag{17}$$

The spin wave energies $\mathcal{E}_k^\gamma = \hbar\omega_k^\gamma$ are found by diagonalizing the matrix $A_k^{\alpha\beta}$. By evaluating the partition function, the free energy can be written in terms of the magnon energies as (N_H is the number of Heisenberg spins)

$$F = -\mathcal{H}_0 + k_B T N \left[\ln 2 + \frac{1}{N_H} \sum_{k,\gamma} \ln(\mathcal{E}_k^\gamma / k_B T)\right]. \tag{18}$$

From the free energy, both entropy S and magnetization M are found by straightforward differentiation.

In the case of the ferromagnetic A2 phase, the lattice is a Bravais lattice (BCC lattice with lattice constant a_0) and then

$$\mathcal{E}_k = B + \sqrt{N_H}(J_0 - J_k) = B + 8J\left[1 - \cos\frac{a_0 k_x}{2}\cos\frac{a_0 k_y}{2}\cos\frac{a_0 k_z}{2}\right]. \tag{19}$$

Thus

$$M|_{B\to 0} = N_H - \frac{k_B T}{8J} \sum_{k\neq 0} \frac{1}{1 - \cos(a_0/2k_x)\cos(a_0/2k_y)\cos(a_0/2k_z)} \tag{20}$$

$$S|_{B\to 0} = -k_B N_H \Bigg\{ \ln(16J/k_B T) - 1 + \frac{1}{N_H} \sum_{k\neq 0} \left[1 - \cos\left(\frac{a_0}{2}k_x\right)\cos\left(\frac{a_0}{2}k_y\right)\cos\left(\frac{a_0}{2}k_z\right)\right] \Bigg\}. \tag{21}$$

Hence the Goldstone mode ($k = 0$) is omitted, since we assert that the symmetry is broken for $B \to 0$, due to the existence of a spontaneous magnetization.

In the case of the B32 phase, the basis cell of the magnetic atoms contains two sites and hence $A_k^{\alpha\beta}$ is a (2×2) matrix,

$$A_k^{\alpha\beta} = \begin{pmatrix} B + 4J & M_k \\ M_k^* & B + 4J \end{pmatrix} \tag{22}$$

where

$$M_k = -J\{1 + \exp[ia_0(k_x - k_z)] + \exp[ia_0(k_x - k_y)] + \exp[ia_0(-k_y - k_z)]\} \tag{23}$$

M_k^* denoting the conjugate complex of M_k. From equations (22) and (23) it is easy to obtain the spin wave energies

$$\mathcal{E}_k^{1,2} = B + 4J\left\{1 \pm \left[\cos^2\left(\frac{a_0}{2}k_x\right)\cos^2\left(\frac{a_0}{2}k_y\right)\cos^2\left(\frac{a_0}{2}k_z\right) + \sin^2\left(\frac{a_0}{2}k_x\right)\sin^2\left(\frac{a_0}{2}k_y\right)\sin^2\left(\frac{a_0}{2}k_z\right)\right]^{1/2}\right\}. \tag{24}$$

This yields for magnetization and entropy

$$M|_{B\to 0} = N_H - \frac{k_B T}{2J}\sum_{k\neq 0}\left\{1 - \cos^2\left(\frac{a_0}{2}k_x\right)\cos^2\left(\frac{a_0}{2}k_y\right)\cos^2\left(\frac{a_0}{2}k_z\right) - \sin^2\left(\frac{a_0}{2}k_x\right)\sin^2\left(\frac{a_0}{2}k_y\right)\sin^2\left(\frac{a_0}{2}k_z\right)\right\}^{-1} \tag{25}$$

$$S|_{B\to 0} = -k_B N_H[\ln(8J/k_B T)] - 1 + \frac{2}{N_H}\sum_{k\neq 0}\ln\left\{1 - \cos^2\left(\frac{a_0}{2}k_x\right)\cos^2\left(\frac{a_0}{2}k_y\right) \times \cos^2\left(\frac{a_0}{2}k_z\right) - \sin^2\left(\frac{a_0}{2}k_x\right)\sin^2\left(\frac{a_0}{2}k_y\right)\sin^2\left(\frac{a_0}{2}k_z\right)\right\}. \tag{26}$$

In the ferromagnetic DO_3 phase we have three spins in the basis cell, and the matrix that needs to be diagonalized reads as follows

$$A_k^{\alpha\beta} = \begin{pmatrix} B + 4J & 0 & M_1(k) \\ 0 & B + 4J & M_2(k) \\ M_1^*(k) & M_2^*(k) & B + 8J \end{pmatrix} \tag{27}$$

where

$$M_1(k) = -J\{1 + \exp[ia_0(k_x - k_z)] + \exp[ia_0(k_x - k_y)] + \exp[ia_0(-k_y - k_z)]\} \tag{28a}$$

$$M_2(k) = -J\{1 + \exp[ia_0(k_x + k_z)] + \exp[ia_0(k_x - k_y)] + \exp[ia_0(-k_y + k_z)]\}. \tag{28b}$$

The resulting spin wave energies are

$$\mathcal{E}_k^1 = B + 4J \tag{29a}$$

$$\mathcal{E}_k^{2,3} = B + 6J \pm 2J\left\{1 + 8\left[\cos^2\left(\frac{a_0}{2}k_x\right)\cos^2\left(\frac{a_0}{2}k_y\right)\cos^2\left(\frac{a_0}{2}k_z\right)\right] + 8\left[\sin^2\left(\frac{a_0}{2}k_x\right)\sin^2\left(\frac{a_0}{2}k_y\right)\sin^2\left(\frac{a_0}{2}k_z\right)\right]\right\}^{1/2}. \tag{29b}$$

From this result magnetization and entropy follow as

$$M|_{B\to 0} = N_H - \frac{k_B T}{4J}\sum_{k\neq 0}\left\{1 + \frac{3}{2}\left[1 - \cos^2\left(\frac{a_0}{2}k_x\right)\cos^2\left(\frac{a_0}{2}k_y\right)\cos^2\left(\frac{a_0}{2}k_z\right) - \sin^2\left(\frac{a_0}{2}k_x\right)\sin^2\left(\frac{a_0}{2}k_y\right)\sin^2\left(\frac{a_0}{2}k_z\right)\right]^{-1}\right\} \tag{30}$$

$$S|_{B\to 0} = -k_B N_H\left\{\ln(8J/k_B T) + \frac{\ln 2}{3} - 1 - \frac{1}{N_H}\sum_{k\neq 0}\ln\left[1 - \cos^2\left(\frac{a_0}{2}k_x\right)\times\cos^2\left(\frac{a_0}{2}k_y\right)\cos^2\left(\frac{a_0}{2}k_z\right) - \sin^2\left(\frac{a_0}{2}k_x\right)\sin^2\left(\frac{a_0}{2}k_y\right)\times\sin^2\left(\frac{a_0}{2}k_z\right)\right]\right\}. \tag{31}$$

Figure 4 shows the temperature dependence of the magnetization for three typical cases, as compared with the Monte Carlo simulation. It is seen that the spin wave approximation is accurate for $k_B T/|V_1| \lesssim 1$.

3.3. Spin wave analysis: quantum-mechanical Heisenberg model

The extension of our treatment to the quantum mechanical case is fairly straightforward, since equations (14)–(17) still remain valid, while equation (18) is replaced by

$$F = -\mathcal{H}_0 + k_B T\sum_{k,j}\ln[1 - \exp(-\mathcal{E}_k^\gamma/k_B T)]. \tag{32}$$

One finds the magnetization and entropy as

$$M|_{B\to 0} = N_H - \sum_{k\neq 0,j}\exp(-\mathcal{E}_k^\gamma/k_B T)/[1 - \exp(-\mathcal{E}_k^\gamma/k_B T)] \tag{33}$$

$$S|_{B\to 0} = k_B\sum_{k\neq 0}\{(\mathcal{E}_k^\gamma/k_B T)\exp(-\mathcal{E}_k^\gamma/k_B T)\}/[1 - \exp(-\mathcal{E}_k^\gamma/k_B T)] - \ln[1 - \exp(-\mathcal{E}_k^\gamma/k_B T)]. \tag{34}$$

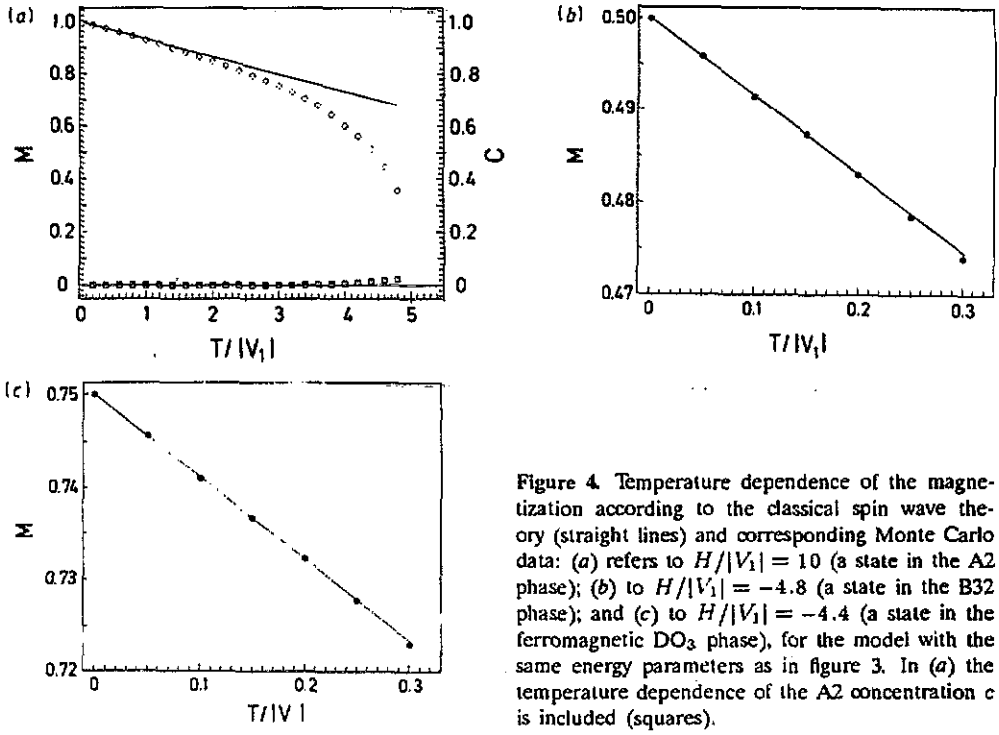

Figure 4. Temperature dependence of the magnetization according to the classical spin wave theory (straight lines) and corresponding Monte Carlo data: (*a*) refers to $H/|V_1| = 10$ (a state in the A2 phase); (*b*) to $H/|V_1| = -4.8$ (a state in the B32 phase); and (*c*) to $H/|V_1| = -4.4$ (a state in the ferromagnetic DO_3 phase), for the model with the same energy parameters as in figure 3. In (*a*) the temperature dependence of the A2 concentration c is included (squares).

Note that equations (19), (24) and (29) describing the spin wave energies in the ferromagnetic A2, B32 and DO_3 phases remain valid. Nevertheless, the low-temperature behaviours of M and S differ drastically from the classical case, as expected: while in the classical case the temperature dependence of M is linear, it now follows the $T^{3/2}$ law; while S in the classical case tends to minus infinity as $T \to 0$, now S tends to zero in agreement with the third law of thermodynamics.

A comparison between the classical and quantum-mechanical low-temperature phase diagram is presented in figure 5. It is seen that the ferromagnetic DO_3 and B32 phases exist up to much higher temperatures in the quantum-mechanical case than in the classical case.

4. Results for the phase diagrams

Following the techniques described by Dünweg and Binder (1987) (see also the appendix of the present paper and Schmid (1991)), mean-field and Monte Carlo phase diagrams were obtained for models I–IV, equations (5)–(8).

Figures 6(*a*) and 6(*b*) show that for model I, the mean-field and Monte Carlo phase diagrams are similar, although the mean-field theory overestimates the transition temperatures to the disordered phase by about a factor 1.5, and the B2–A2 phase boundary according to the simulation lacks the re-entrancy predicted by the mean field calculation. As has already been shown in figure 5(*b*), the low-temperature part of the mean-field phase diagram is in excellent agreement with the Monte Carlo data. It is remarkable that, although the B2 phase exists over a very wide range of T

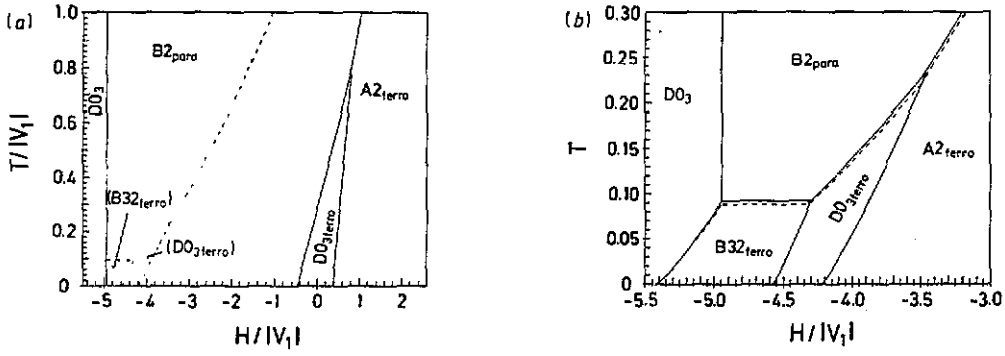

Figure 5. (*a*) Grand-canonical phase diagram in the T–H plane at low temperatures according to the quantum-mechanical spin wave approximation (full curves) and the spin wave approximation for classical spins (broken curves), for model I (equation (5)). The nature of the various phases is indicated in the figure. Note that $J/|V_1| = 2.5$ in the classical case, but $J/|V_1| = 1.35$ in the quantum case. (*b*) same as (*a*), but classical spin wave approximation (full curves) compared with the mean-field approximation (broken curves).

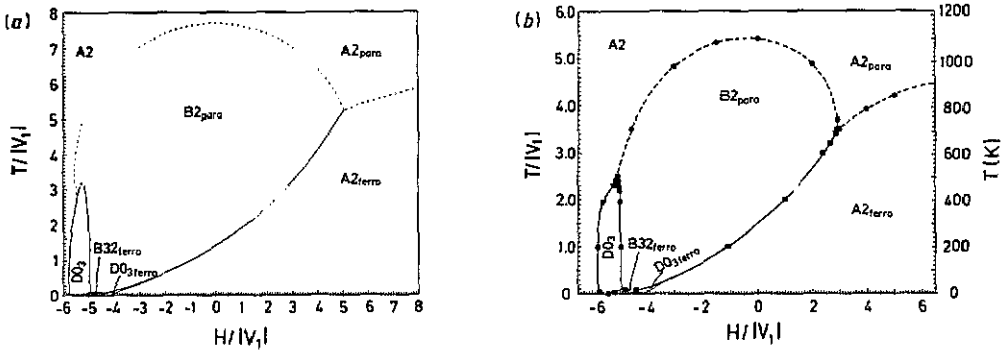

Figure 6. Grand-canonical phase diagram of model I in the T–H plane according to mean-field (*a*) and Monte Carlo (*b*) calculations. Second-order transitions are shown as broken curves, while first-order transitions are shown as full curves. The nature of the various phases is indicated in the figure.

and H, it is not the stable equilibrium phase for very low T, where the B32 phase takes over instead.

Translating this phase diagram from the grand-canonical ensemble of the alloy appropriately to the canonical ensemble (figure 7), comparison with the experimental results (figure 1) reveals a striking dissimilarity: clearly the B2 phase should be stable up to much higher temperatures than observed in figure 7, the ferromagnetic Fe_3Al phase is also missing, and the coexistence region between the ferromagnetic A2 and B2 phases is far too wide in figure 7. The same problems occur for model II, figure 8—the main distinction being that for model II the B2 phase remains the stable down to $T = 0$.

Thus, although both models I and II are supported by experimental results (table 1), they are not capable of reproducing the correct phase diagram. While the magnetic interaction was adjusted in order to enforce the correct transition tempera-

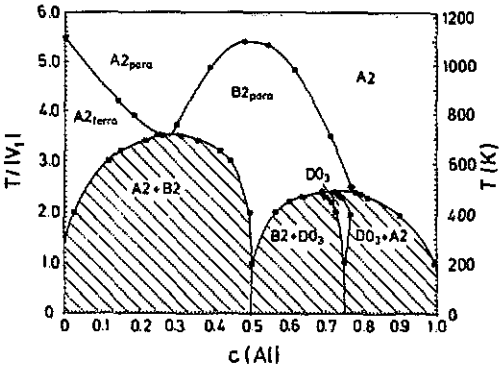

Figure 7. Canonical phase diagram of model I as obtained from the Monte Carlo simulation. Two-phase coexistence regions are shaded. Note that the ferromagnetic DO_3 and B32 phases and corresponding two-phase regions, which are not stable for $T/|V_1| \gtrsim 0.25$, are omitted in this figure.

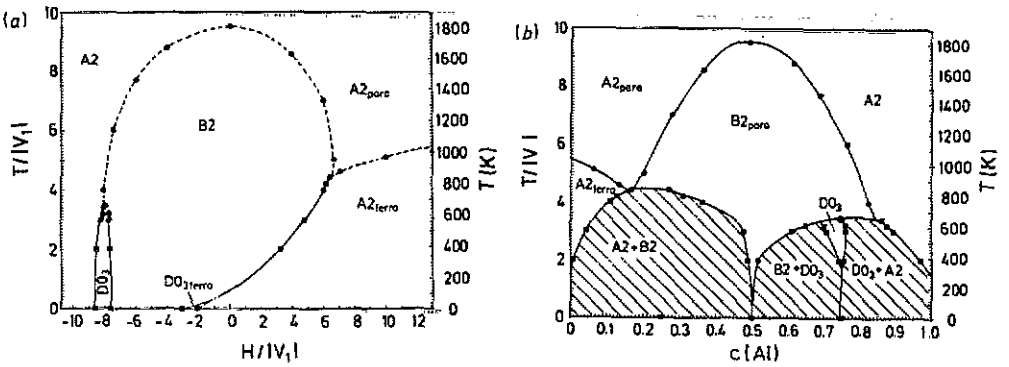

Figure 8. Grand-canonical (*a*) and canonical (*b*) phase diagram of model II (equation (6)). Again in (*a*) second-order transition lines are shown as broken curves, while first-order transitions are shown in full, and in (*b*) two-phase coexistence regions are shaded.

ture between the ferro- and para-magnetic A2 phases as the Al content goes to zero, it is obvious that transition temperatures of the A2–B2 order–disorder transition for Al concentrations near $c_{Al} \approx 30\%$ are severely underestimated. Consequently, models I and II suffer from the ratio of magnetic-to-crystallographic interactions being too large (with respect to its absolute value). As an extreme example of a model with a weak magnetic interaction, we treated model III (equation (7), see figure 9): now the Fe_3Al phase would exist up to temperatures about as high as those of the $FeAl_3$ phase. It is clear, however, that for this model the magnetic interaction is too weak, since ferromagnetic A2 and DO_3 phases only exist at extremely low temperatures.

In view of this observation, it seems best to treat the ratio between magnetic and crystallographic interaction as an adjustable parameter, rather than the absolute strength of the magnetic exchange. This consideration motivates the choice of model IV, equation (8), and indeed figures 10 and 11 reveal satisfactory behaviour. We recognize that the topology of the experimental phase diagram (figure 1) on the iron-rich side and the topology of figure 11 are the same—a coexistence region between the ferromagnetic A2 phase and the paramagnetic FeAl phase (B2 structure) exists underneath the bicritical point. (This is the first time that a model calculation has reproduced this feature of the phase diagram.) Both ferromagnetic and paramagnetic Fe_3Al phases occur, separated by a critical line. This line terminates at critical end

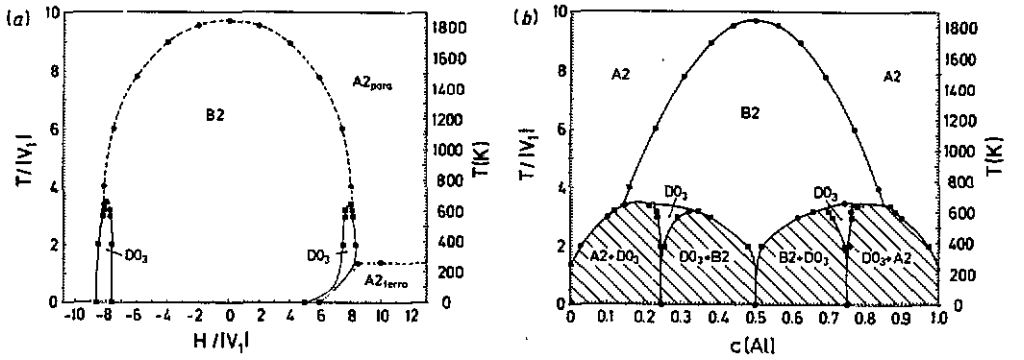

Figure 9. Grand-canonical (*a*) and canonical (*b*) phase diagram of model III (equation (7)).

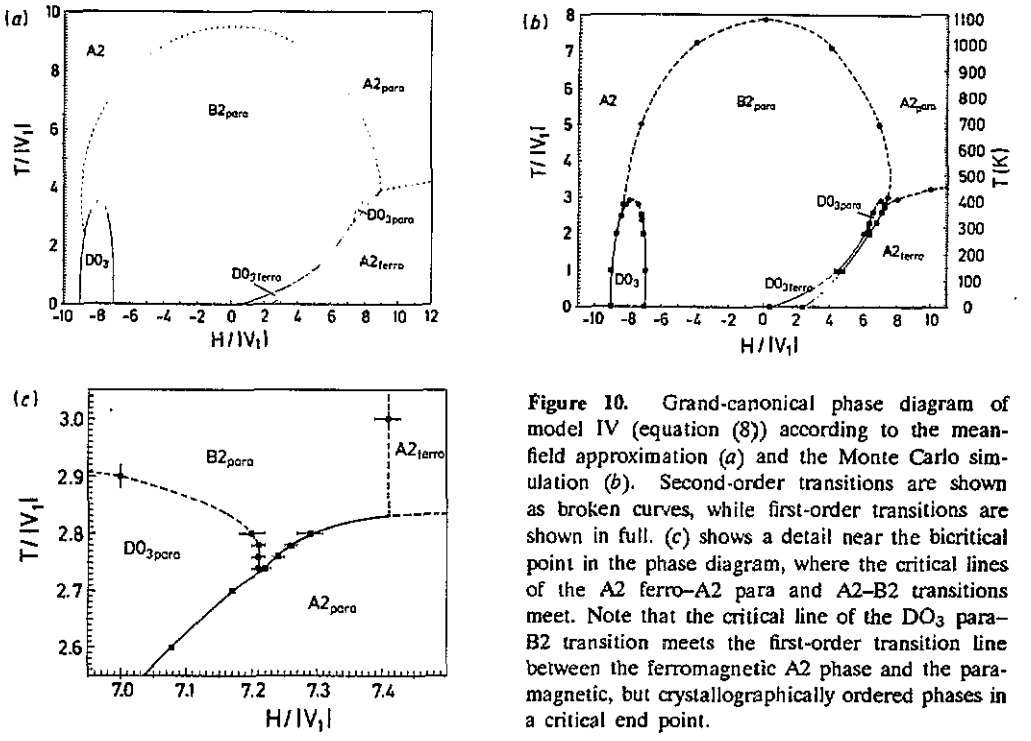

Figure 10. Grand-canonical phase diagram of model IV (equation (8)) according to the mean-field approximation (*a*) and the Monte Carlo simulation (*b*). Second-order transitions are shown as broken curves, while first-order transitions are shown in full. (*c*) shows a detail near the bicritical point in the phase diagram, where the critical lines of the A2 ferro–A2 para and A2–B2 transitions meet. Note that the critical line of the DO_3 para–B2 transition meets the first-order transition line between the ferromagnetic A2 phase and the paramagnetic, but crystallographically ordered phases in a critical end point.

points on both sides—in the experimental phase diagram the low-temperature part of this line is unknown, of course, since for $T \lesssim 200°$ Fe–Al alloys are no longer in thermal equilibrium. Also the tricritical point where the second-order DO_3–B2 transition ends can perhaps be associated with an experimentally observed feature (interpreting the 'K2 phase' in figure 1 as a two-phase region between the Fe_3Al and FeAl phases).

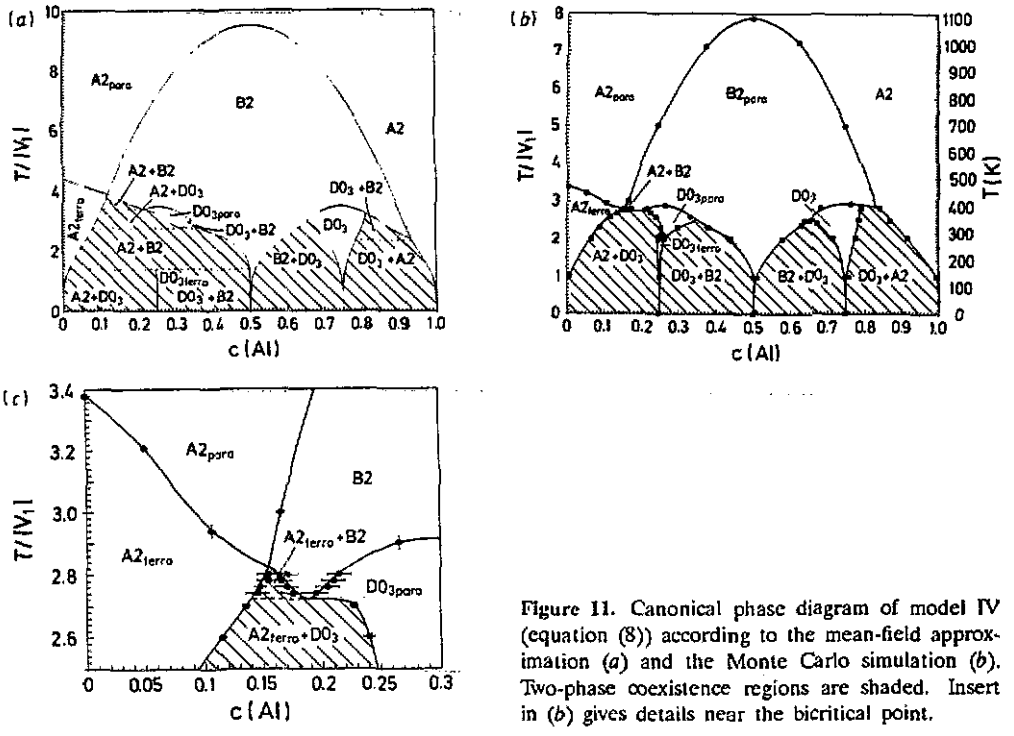

Figure 11. Canonical phase diagram of model IV (equation (8)) according to the mean-field approximation (*a*) and the Monte Carlo simulation (*b*). Two-phase coexistence regions are shaded. Insert in (*b*) gives details near the bicritical point.

5. Discussion

In this paper, we have taken the interaction parameters extracted from scattering experiments from $Fe_{0.8}Al_{0.2}$ alloys and tried to use them to predict the iron-rich part of the phase diagram by Monte Carlo simulation. While the result is even qualitatively very different from reality when these interaction parameters are used in conjunction with an exchange constant fitted to the Curie temperature of pure iron, a qualitatively reasonably phased diagram results from treating the ratio of magnetic and crystallographic interactions as an adjustable parameter. The comparison between simulation (figure 11(*b*)) and experiment (figure 1) still reveals significant differences between the quantitative location of various transition lines in the temperature–composition plane. As a consequence, we must conclude that our knowledge of effective interactions in Fe–Al alloys is still not completely satisfactory. What would, in our opinion, be needed to clarify the situation are the following studies:

(i) Simultaneous measurements of both crystallographic and magnetic short-range order (e.g. by polarized neutron scattering analysis) to estimate all effective interaction parameters in a coherent manner from one set of experimental data;

(ii) Measurements at several Al concentrations (in the range of 10 to 35% Al content) to clarify whether it is a good approximation to take the effective interaction parameters independent of concentration;

(iii) Simulation of order–disorder transitions in models which have full lattice-dynamical degrees of freedom, thus allowing at least for the different lattice spacings (and possibly also different lattice structures) of Fe and Al. It is possible that local

elastic distortions already play an important role, even on the iron-rich side of the phase diagram.

(iv) Treatment of the magnetic degree of freedom of iron by quantum Monte Carlo methods (within the framework of Heisenberg as well as Hubbard models).

Clearly, all these studies would be very demanding—and some of them may not even be feasible at this time. Thus, although the long-term prospects of a better understanding ordering phenomena in alloys by computer simulation are very interesting, there are still challenging problems that need to be overcome. We hope that the present work will also stimulate interest in other suitable alloys, so that more measurements of effective interaction parameters become available, providing a broader test of corresponding models.

Acknowledgments

We are grateful to W Schweika and V Pierron-Bohnes for information on their measurements of interaction parameters prior to publication. One of us (FS) received support under the Landesgraduierten-Förderungsgesetz Rheinland-Pfalz. This work was carried out using extensive computer time at the Siemens-Fijitsu VP100 computer at the Regionales Hochschulrechenzentrum Kaiserslautern (RHRK).

Appendix. Comment on the mean-field approximation

In a mean-field or Bragg–Williams approximation, mean concentrations and magnetizations on a specified sublattice a, b, c or d (see figure 2(*a*)) are determined by the effective mean chemical field $H^{\text{eff}}_{\text{a,b,c,d}}$ and magnetic field $B^{\text{eff}}_{\text{a,b,c,d}}$ acting on a particle in this sublattice.

From (1) one gets

$$H^{\text{eff}}_{\alpha} = H^{0}_{\alpha} + H \qquad (\alpha = \text{a,b,c,d}) \tag{A1}$$

with

$$H^{0}_{\text{a}} = (4V_1 + 12V_4)(\langle S_{\text{c}}\rangle + \langle S_{\text{d}}\rangle) + 6V_2\langle S_{\text{b}}\rangle + 12V_3\langle S_{\text{a}}\rangle$$
$$H^{0}_{\text{b}} = (4V_1 + 12V_4)(\langle S_{\text{c}}\rangle + \langle S_{\text{d}}\rangle) + 6V_2\langle S_{\text{a}}\rangle + 12V_3\langle S_{\text{b}}\rangle$$
$$H^{0}_{\text{c}} = (4V_1 + 12V_4)(\langle S_{\text{a}}\rangle + \langle S_{\text{b}}\rangle) + 6V_2\langle S_{\text{d}}\rangle + 12V_3\langle S_{\text{c}}\rangle$$
$$H^{0}_{\text{d}} = (4V_1 + 12V_4)(\langle S_{\text{a}}\rangle + \langle S_{\text{b}}\rangle) + 6V_2\langle S_{\text{c}}\rangle + 12V_3\langle S_{\text{d}}\rangle$$

and

$$B^{\text{eff}}_{\alpha} = B^{0}_{\alpha} \tag{A2}$$

$$B^{0}_{\text{a}} = B^{0}_{\text{b}} = 4J\left(\langle\sigma_{\text{c}}\rangle\frac{1+\langle S_{\text{c}}\rangle}{2} + \langle\sigma_{\text{d}}\rangle\frac{1+\langle S_{\text{d}}\rangle}{2}\right)$$

$$B^{0}_{\text{c}} = B^{0}_{\text{d}} = 4J\left(\langle\sigma_{\text{a}}\rangle\frac{1+\langle S_{\text{a}}\rangle}{2} + \langle\sigma_{\text{b}}\rangle\frac{1+\langle S_{\text{b}}\rangle}{2}\right).$$

The partition function of a single lattice site in a field H^{eff}, B^{eff} is given by

$$Z = \mathrm{e}^{-\beta H^{\text{eff}}} + \mathrm{e}^{\beta H^{\text{eff}}} \frac{1}{2\beta B^{\text{eff}}} (\mathrm{e}^{\beta B^{\text{eff}}} - \mathrm{e}^{-\beta B^{\text{eff}}}) \tag{A3}$$

This leads to the mean-field equations:

$$\langle S_\alpha \rangle = \frac{1}{Z} \left\{ -\mathrm{e}^{-\beta H_\alpha^{\text{eff}}} + \mathrm{e}^{\beta H_\alpha^{\text{eff}}} \frac{1}{2\beta B_\alpha^{\text{eff}}} (\mathrm{e}^{+\beta B_\alpha^{\text{eff}}} - \mathrm{e}^{-\beta B_\alpha^{\text{eff}}}) \right\} \tag{A4a}$$

$$\langle \sigma_\alpha \rangle \left(\frac{1 + \langle S_\alpha \rangle}{2} \right) = \frac{1}{Z} \mathrm{e}^{\beta H_\alpha^{\text{eff}}} \frac{1}{2} \left\{ \left(\frac{1}{\beta B_\alpha^{\text{eff}}} - \frac{1}{(\beta B_\alpha^{\text{eff}})^2} \right) \mathrm{e}^{\beta B_\alpha^{\text{eff}}} + \left(\frac{1}{\beta B_\alpha^{\text{eff}}} + \frac{1}{(\beta B_\alpha^{\text{eff}})^2} \right) \mathrm{e}^{-\beta B_\alpha^{\text{eff}}} \right\} \frac{B_\alpha^{\text{eff}}}{B_\alpha^{\text{eff}}} \tag{A4b}$$

which can be solved numerically.

Note that symmetry considerations may considerably reduce the number of equations. Since magnetic interaction is purely ferromagnetic, e.g. the mean magnetizations $\langle \sigma_\alpha \rangle$ will always point in the same direction and the vectors in equations (A2) and (A4*b*) might as well be replaced by scalars.

Given different solutions of equation (A4), one still has to evaluate the free energy in order to determine its absolute minimum. The internal energy is given by

$$U/(N/4) = -\tfrac{1}{2} \sum_\alpha H_\alpha^0 \langle S_\alpha \rangle - \tfrac{1}{2} \sum_\alpha B_\alpha^0 \langle \sigma_\alpha^0 \rangle (1 + \langle S_\alpha \rangle)/2 - H \sum_\alpha \langle S_\alpha \rangle \tag{A5}$$

and the entropy due to chemical disorder

$$S_{\text{chem}}/(N/4) = -\sum_\alpha \left[\frac{1 + \langle S_\alpha \rangle}{2} \ln \left(\frac{1 + \langle S_\alpha \rangle}{2} \right) + \frac{1 - \langle S_\alpha \rangle}{2} \ln \left(\frac{1 - \langle S_\alpha \rangle}{2} \right) \right]. \tag{A6}$$

To find an expression for the entropy due to magnetism is slightly more difficult. If one considers a system of N non-interacting Heisenberg spins in a magnetic field B, one gets the magnetization and entropy

$$\langle \sigma \rangle (u) = N \frac{\mathrm{e}^u (u - 1) + \mathrm{e}^{-u} (u + 1)}{u (\mathrm{e}^u - \mathrm{e}^{-u})} \tag{A7a}$$

$$S(u) = N k_{\text{B}} \ln \left[\frac{1}{2u} (\mathrm{e}^u - \mathrm{e}^{-u}) \right] - k_{\text{B}} u \langle \sigma \rangle (u) \tag{A7b}$$

with $u = B/k_{\text{B}}T$.

As the function $\langle \sigma \rangle (u)$ increases monotonically, this defines an inverse function of $u(\langle \sigma \rangle)$ and therefore an entropy function $\tilde{S}(\langle \sigma \rangle) \equiv S(u(\langle \sigma \rangle))$. Thus the entropy due to magnetism turns out to be

$$S_{\text{magn}}/(N/4) = \sum_\alpha \frac{1 + \langle S_\alpha \rangle}{2} \tilde{S}(\langle \sigma_\alpha \rangle). \tag{A8}$$

One finally arrives at the total free energy

$$F = U - T(S_{\text{magn}} + S_{\text{chem}}). \tag{A9}$$

References

Ackermann H, Crusius S, and Inden G 1986 *Acta Metall.* **34** 2311
Ackermann H, Crusius S, and Kikuchi R 1989 *Acta Metall.* **37** 1
Allen S M 1977 *Phil. Mag.* **36** 181
Allen S M and Cahn J W 1975 *Acta Metall.* **23** 1017
—— 1976 *Acta Metall.* **24** 425
Beck P A 1971 *Metal Trans.* **2** 2015
Bieber A and Gautier F 1984a *Z. Phys.* B **57** 335
—— 1984b *J. Phys. Soc. Japan* **53** 2061
Binder K 1980 *Phys. Rev. Lett.* **45** 811
—— 1981 *Z. Phys.* B **45** 61
—— 1986 *Festkörperprobleme (Advances in Solid State Physics 26)* ed P Grosse (Braunschweig: Vieweg) p 133
Bradley A I and Jay A H 1932 *Proc. R. Soc.* A **136** 210
Cable J W, David C and Parra R 1977 *Phys. Rev.* B **16** 1132
Carlsson A E 1987 *Phys. Rev.* B **35** 4858
—— 1988 *Phys. Rev.* B **40** 912
Colinet C, Inden G, and Kikuchi R 1992 *Acta Metall.* to appear
Collins M F, Minkiewicz V J, Nathans R, Passell and Shirane G 1969 *Phys. Rev.* **179** 417
Contreras-Solorio D A, Mejša-Lira F, Moran-Lopéz J L and Sanchez J M 1988 *Phys. Rev.* B **38** 11481
—— 1988 *J. Physique Coll.* **49** C8 105
Davies R G 1953 *J. Phys. Chem. Sol.* **24** 985
De Fontaine D 1979 *Solid State Physics* vol 34, ed H Ehrenreich, F Seitz and D Turnbull (New York: Academic)
Diep H T, Ghazali A, Berge B and Lallemand P 1986 *Europhys. Lett.* **2** 603
Domb C 1974 *Phase Transitions and Critical Phenomena* vol 3, ed C Domb and M S Green (London: Academic)
Dünweg B and Binder K 1987 *Phys. Rev.* B **36** 6935
Finel A and Ducastelle F 1986 *Europhys. Lett.* **1** 135
Friedmann E A and Nicholson W 1963 *J. Appl. Phys.* **34** 1048
Gahn U 1982 *J. Phys. Chem. Solids* **43** 977
—— 1986 *J. Phys. Chem. Solids* **47** 1153
Gautier F, Ducastelle F and Giner J 1975 *Phil. Mag.* **31** 1373
Gerold V and Kern J 1987 *Acta Metall.* **35** 393
Gonis A, Zhang X G, Freeman A J, Turchi P, Stocks G M and Nicholson D M 1987 *Phys. Rev.* B **36** 4630
Gonis A, Turchi P, Zhang X G, Stocks G M, Nicholson D M and Butler W H 1989 *Atomistic Simulation of Materials* ed V Vitek and D J Srolovik (New York: Plenum) p 15
Gyorffy B L and Stocks G M 1983 *Phys. Rev. Lett.* **50** 374
Inden G 1983 *Mater. Res. Soc. Symp. Proc.* vol 19 (New York: Elsevier) p 175
Inden G and Pepperhoff W 1990 *Z. Metall.* **81** 770
Inden G and Pitsch W 1991 *Materials Science and Technology, vol 5: Phase Transformations in Materials* ed P Haasen (Weinheim: VCH) p 497
Khachaturyan A G 1978 *Progress in Materials Science* vol 22 (New York: Pergamon) p 1
Kikuchi R 1974 *J. Chem. Phys.* **60** 1071
Kikuchi R and van Baal C M 1974 *Scr. Metall.* **8** 425
Köster W and Gödecke T 1980 *Z. Metall.* **71** 765
—— 1981 *Z. Metall.* **72** 569
—— 1982 *Z. Metall.* **73** 111
Kubaschewski O 1982 *Iron-Binary Phase Diagrams* (Berlin: Springer) p 5
Kuentzler R 1983 *J. Physique* **44** 1167

Loong C K, Carpenter J M, Lynn J W, Robinson H A and Mook H A 1984 *J. Appl. Phys.* **55** 1895
Min B I, Oguchi T, Jansen H J F and Freeman A J 1986 *J. Magn. Magn. Mater.* **54–57** 1091
Mohri T, Sanchez J M and De Fontaine D 1985 *Acta Metall.* **33** 1171
Nathans R, Pigott M T and Skull C G 1958 *J. Phys. Chem. Solids* **6** 38
Okamoto H and Beck P A 1971 *Metal Trans.* **2** 569
Pickart S J and Nathans R 1961 *Phys. Rev.* **123** 1163
Pierron-Bohnes V, Cadeville M C, Finel A and Schaerpf O 1991a *J. Physique* **I1** 247
Pierron-Bohnes V, Lefevbre S, Bessiere M and Finel A 1991b *Acta Metall.* **38** 2701
Rushbrooke G S, Baker G A Jr and Wood P J 1974 *Phase Transitions and Critical Phenomena* vol 3, ed C Domb and M S Green (London: Academic)
Sagane K and Oki K 1980 *Trans. Japan. Inst. Met.* **21** 12
Sanchez J M and De Fontaine D 1978 *Phys. Rev.* B **17** 2926
—— 1980 *Phys. Rev.* B **21** 216
—— 1982 *Phys. Rev.* B **25** 1759
Schmid F 1991 *Dissertation* Johannes Gutenberg Universität Mainz, unpublished
Schweika W 1990 *Mat. Res. Soc. Symp. Proc.* **166** 249
Semenovskaya V 1974 *Phys. Status Solidi* b **64** 291
Shiba M and Nakamura Y 1976 *J. Phys. Soc. Japan* **40** 1295
Shukla P and Wortis M 1980 *Phys. Rev.* B **21** 159
Shull R D, Okamoto H and Beck P A 1976 *Solid State Commun.* **20** 863
Stocks G M and Gonis A (eds) 1989 *Alloy Phase Stability* (Dordrecht: Kluwer)
Swann P R, Duff W R and Fisher R M 1972 *Metal Trans.* **3** 409
Thomas H 1950 *Z. Metall.* **41** 185
—— 1951 *Z. Phys.* **129** 219
Turchi P, Treglia G and Ducastelle F 1983 *J. Phys. F: Met. Phys.* **13** 2543
Warlimont H and Thomas G 1974 *Metal Soc. J.* **4** 47